

THEORY OF “JITTER” RADIATION FROM SMALL-SCALE RANDOM MAGNETIC FIELDS AND PROMPT EMISSION FROM GAMMA-RAY BURST SHOCKS

MIKHAIL V. MEDVEDEV¹

Harvard-Smithsonian Center for Astrophysics, 60 Garden Street, Cambridge, MA 02138

Draft version October 27, 2018

ABSTRACT

We demonstrate that the radiation emitted by ultrarelativistic electrons in highly nonuniform, small-scale magnetic fields is different from synchrotron radiation if the electron’s transverse deflections in these fields are much smaller than the beaming angle. A quantitative analytical theory of this radiation, which we refer to as jitter radiation, is developed. It is shown that the emergent spectrum is determined by statistical properties of the magnetic field. The jitter radiation theory is then applied to internal shocks of Gamma-Ray Bursts (GRBs). The model of a magnetic field in GRBs (Medvedev & Loeb 1999, ApJ, 526, 697) is used. The spectral power distribution of radiation produced by the power-law distributed electrons with a low-energy cutoff is well described by a sharply broken power-law: $P(\omega) \propto \omega^1$ for $\omega \lesssim \omega_{jm}$ and $P(\omega) \propto \omega^{-(p-1)/2}$ for $\omega \gtrsim \omega_{jm}$, where p is the electron power-law index and ω_{jm} is the jitter break frequency which is independent of the field strength but depends on the electron density in the ejecta, $\omega_{jm} \propto \sqrt{n}$, as well as on the shock energetics and kinematics. The total emitted power of jitter radiation is, however, equal to that of synchrotron radiation.

Since large-scale fields may also be present in the ejecta, we construct a two-component, jitter+synchrotron spectral model of the prompt γ -ray emission. Quite surprisingly, this model seems to be readily capable of explaining several properties of time-resolved spectra of some GRBs, such as (i) the violation of the constraint on the low-energy spectral index called the synchrotron “line of death”, (ii) the sharp spectral break at the peak frequency, inconsistent with the broad synchrotron bump, (iii) the evidence for two spectral sub-components, and (iv) possible existence of emission features called “GRB lines”. We believe these facts strongly support both the existence of small-scale magnetic fields and the proposed radiation mechanism from GRB shocks. As an example, we use the composite model to analyze GRB 910503 which has two spectral peaks. At last, we emphasize that accurate GRB spectra may allow precise determination of fireball properties as early as several minutes after the explosion.

Subject headings: radiation mechanisms: non-thermal — gamma rays: bursts — magnetic fields

1. INTRODUCTION

The conventional paradigm of the generation of radiation by relativistic electrons in magnetic fields is totally based on the theory of synchrotron radiation. We demonstrate that this theory is invalid if a magnetic field is tangled on very short spatial scales and we develop a quantitative theory of radiation in this case. Apparently, the required short-scale fields may naturally be present in astrophysical shocks. Here we focus on radiation from gamma-ray burst (GRB) shocks, for which a detailed theory of the formation of magnetic fields has recently been elaborated.

The relativistic blast-wave model of cosmological GRBs (see, e.g., a review by Piran 1999) explains fairly well many observational features of this phenomenon, such as the rapid variability of γ -ray flux, the prompt optical flash, the light curves and spectra of delayed afterglows, etc.. This model interprets the prompt γ -ray flash as synchrotron radiation emitted by Fermi-accelerated electrons in internal shocks propagating in the ejecta (Rees & Mészáros 1994) and then Lorentz-boosted to the γ -ray band. The afterglows are explained in a similar way, as the emission from an external shock (Mészáros & Rees 1993) propagating into the interstellar medium. To achieve the observed very high luminosities, the magnetic field in the

GRB shocks must be of nearly equipartition strength, $\epsilon_B = B^2/8\pi e_t \sim 1$, where e_t is the thermal energy density of the shocked material.

Until very recently, the equipartition assumption was completely unjustified. Medvedev & Loeb (1999) have shown that the relativistic two-stream instability is capable of producing magnetic fields with $\epsilon_B \sim 10^{-1} - 10^{-5}$ in both internal and external shocks. Observations of afterglow spectra and light curves yield values of ϵ_B from $\sim 10^{-1} - 10^{-2}$ for GRB 970508 (Wijers & Galama 1998; Frail et al. 1999; Granot et al. 1999) to $\sim 10^{-5}$ for GRB 990123 and GRB 971214 (Galama et al. 1999). Recent detection of polarization of the optical afterglow of GRB 990510 (Covino et al. 1999; Wijers et al. 1999) indicates that the geometry of the magnetic field in the shock is consistent with the predictions of Medvedev & Loeb (1999) for collimated outflows (Ghisellini & Lazzati 1999; Gruzinov 1999; Sari 1999).

The magnetic field produced in GRB shocks randomly fluctuates on a very small scale of roughly the relativistic skin depth, which is $\lambda_B \sim 10^2$ cm in internal shocks, for instance. On the other hand, the emitting ultrarelativistic electrons have much larger Larmor radii. Therefore, the electron trajectories are not helical, as they would be in a

¹Also at the Institute for Nuclear Fusion, RRC “Kurchatov Institute”, Moscow 123182, Russia; mmedvedev@cfa.harvard.edu; <http://cfa-www.harvard.edu/~mmedvede/>

homogeneous field. Thus, the theory of synchrotron radiation derived for homogeneous fields is not applicable and the spectrum of the emergent radiation is different. Such a situation has never been considered in the astrophysical literature.

In this paper we investigate the effect of small-scale magnetic fields on the properties of radiation. We primarily focus on internal shocks, for concreteness. We show that there are two regimes, depending on the ratio of particle's deflection angle and the relativistic beaming angle. Which regime is realized depends on the magnetic field properties, B and λ_B , but is independent of the particle's energy. When deflections are large compared to beaming, synchrotron radiation is emitted. Otherwise, when particle's deflections are small, a new type of radiation — jitter radiation — is produced. A quantitative analytical theory of this radiation is developed in this paper. For the power-law distributed electrons with a cutoff, $N(\gamma) \propto \gamma^{-p}$ for $\gamma \geq \gamma_{\min}$, where γ is the particle's Lorentz factor and p is the index, the emergent spectrum has the following properties. First, the spectral power peaks at the so-called jitter frequency, $\omega_{jm} = \omega_j(\gamma_{\min})$, which, unlike the synchrotron frequency, is independent of the magnetic field strength but, instead, depends on the particle density in the shock, $\omega_{jm} \propto \sqrt{n}$. Second, at low frequencies, $\omega \leq \omega_{jm}$, the spectral power scales as $P(\omega) \propto \omega^1$, in contrast to the synchrotron spectrum, for which $P(\omega) \propto \omega^{1/3}$. The high-frequency portion is, however, determined by the electrons, $P(\omega) \propto \omega^{-(p-1)/2}$. Third, the total (i.e., frequency integrated) powers emitted in the jitter and synchrotron regimes are identical.

Since large-scale fields (e.g., due to a magnetized progenitor, for instance) may also be present in the shocked material, we construct a composite, two-component jitter+synchrotron (JS) spectral model of the prompt γ -ray emission. We then compare the predictions of this model with presently available data collected (mostly) by the Burst And Transient Source Experiment (BATSE) on the *Compton Gamma-Ray Observatory (CGRO)*. It turns out that the JS model is able to naturally explain some properties of the GRB spectra which are inconsistent with a simple synchrotron shock model. First, almost a half of all BATSE bursts violate the so-called synchrotron “line of death” prediction, i.e., their low-frequency spectral indices are greater than the maximal admissible value of $1/3$ (Preece et al. 1998). The spectra of these bursts are, however, well consistent with the steeper ω^1 -law of jitter radiation. Second, the sharp change of the spectral index at a peak frequency seen in some bursts is also consistent with our model. Third, the JS model theoretically supports the fact that some GRBs have two spectral sub-components (Pendleton et al. 1994). Fourth, there is an indication that spectra of some GRBs exhibit spectral features — “GRB lines” (see Briggs 1999 for a review and some BATSE candidates). It should be noted, however, that the results from *Ginga* and BATSE are somewhat controversial. We demonstrate that a line-like spectral feature may be associated with a weak jitter component in a synchrotron-dominated spectrum. If a future analysis shall confirm that “GRB lines” are real features and not instrumental (or other) artifacts, then they provide, together with the synchrotron component, precise informa-

tion about properties of cosmological fireballs just a few hundred seconds after the explosion. We illustrate this on the example of GRB 910503 which has been observed by all four instruments on the *CGRO* and which exhibits a second spectral peak at roughly twice the synchrotron peak frequency. A simple fit of a spectral shape readily yields the value of the magnetic field, $\epsilon_B \sim 4 \times 10^{-4}$ in the shock, which is in agreement with results of a completely different analysis by Chiang & Dermer (1999). It should be noted that a reliable identification/detection of the jitter spectral features will provide a direct evidence that the magnetic fields in GRBs are generated by the two-stream instability, since this is the only presently known mechanism capable of producing small-scale, large-amplitude fields in shocks.

At last, we emphasize that the advantage of our JS model is that it was *not* specially designed in order to explain peculiarities of the GRB spectra, but solely to study the physical effect of small-scale magnetic fields. The phenomenon considered in this paper is quite general and, clearly, relevant not only to the emission from internal GRB shocks. A similar mechanism of emission is expected to operate in external GRB shocks and, possibly, in more conventional supernova shocks and blazar jets.

The rest of this paper is organized as follows. A qualitative consideration of the radiation mechanisms in a nonuniform magnetic field is presented in §2. In §3 the structure and properties of magnetic fields in GRB internal shocks are discussed. In §4 we present a quantitative analytical theory of jitter radiation. A two-component, jitter+synchrotron spectral model of the prompt γ -ray emission is presented in §5. We compare the predictions of the model with recent observational results in §6. Finally, §7 is the conclusion.

2. RADIATION FROM SMALL-SCALE FIELDS: GENERAL CONSIDERATION

Let's consider a plasma at rest threaded by a magnetic field. Let's now consider an ultrarelativistic electron with the Lorentz factor $\gamma \gg 1$ moving in a magnetic field. Because of beaming the emerging radiation is concentrated in a narrow cone with the opening angle $\Delta\theta \sim 1/\gamma \ll 1$ in the direction of the particle's velocity. In a uniform magnetic field the electron moves along a helical trajectory, so that the radiation seen by an observer consists of short pulses repeated every cyclotron period. The synchrotron spectrum, therefore, consists of a large number of cyclotron harmonics, the envelope of which is determined by the inverse duration of the pulses (Rybicki & Lightman 1979). The spectrum is peaked near the critical synchrotron frequency $\omega_c = \frac{3}{2}\gamma^2 eB_{\perp}/m_e c$, where $B_{\perp} = B \cos \chi$ and χ is the particle's pitch angle.

If the magnetic field is randomly tangled and the correlation length is less than a Larmor radius of an emitting electron, then the electron experiences random deflections as it moves through the field. Its trajectory is, in general, stochastic. This is similar to a collisional motion of an electron in a medium. Bremsstrahlung quanta are emitted in every collision. Unlike the bremsstrahlung case, here “collisions” are due to small-scale inhomogeneities of the magnetic field rather than due to electrostatic fields of other charged particles. Since the Lorentz force depends on particle's velocity, the emergent spectrum will be some-

what different from pure bremsstrahlung. There is also an alternative physical interpretation of the process. For an ultrarelativistic electron, the method of virtual quanta applies (Rybicki & Lightman 1979). In the rest frame of the electron, the magnetic field inhomogeneity with wavenumber k is transformed into a transverse pulse of electromagnetic radiation with frequency kc . This radiation is then Compton scattered by the electron to produce observed radiation with frequency $\sim \gamma^2 kc$ in the lab frame.

Keeping this general physical picture in mind, we now analyze the problem in more details. Let's consider a nonuniform random magnetic field with a typical correlation scale λ_B , the Larmor radius of the electron, $\rho_e = \gamma m_e c^2 / e B_\perp$ is less or comparable to λ_B . The emerging spectrum depends on the relation between the particle's deflection angle, α , and the beaming angle, $\Delta\theta$, (Landau & Lifshits 1975). For ultrarelativistic particles and small deflection angles, the latter is estimated as follows. The particle's momentum is $p \sim \gamma m_e c$. The change in the perpendicular momentum due to the Lorentz force acting on the particle during the transit time $t \sim \lambda_B / c$ is $p_\perp \sim F_L t \sim e B_\perp \lambda_B / c$. The angle α is then $\alpha \sim p_\perp / p \sim e B_\perp \lambda_B / \gamma m_e c^2$. Thus, the ratio of the two angles is

$$\frac{\alpha}{\Delta\theta} \sim \frac{e B_\perp \lambda_B}{m_e c^2} \sim \gamma \frac{\lambda_B}{\rho_e}. \quad (1)$$

It is interesting to note that this ratio is independent of particle's energy (i.e., of γ) and is determined by the properties of the magnetic field only, i.e., by B and λ_B . It is more convenient, however, to use the wave-vector, k_B , as a measure of the magnetic field scale, instead of $\lambda_B \sim k_B^{-1}$. We now define the deflection-to-beaming ratio as follows,

$$\delta \equiv \frac{\gamma}{k_B \rho_e} \sim \frac{\alpha}{\Delta\theta}. \quad (2)$$

There are two limiting cases.

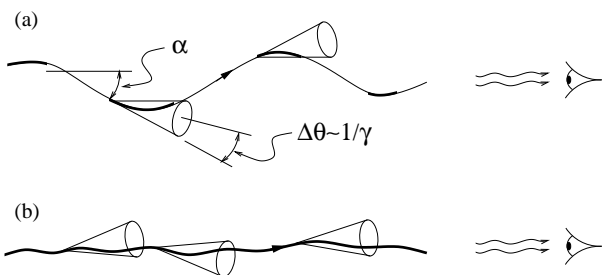


FIG. 1.— Emission from various points along particle's trajectory; (a) — $\alpha \gg \Delta\theta$, emission from selected parts (bold portions) of the trajectory is seen by an observer, (b) — $\alpha \ll \Delta\theta$, emission from the entire trajectory is observed.

First, $\delta \sim \alpha / \Delta\theta \gg 1$, i.e., the deflection angle is much larger than the beaming angle, see Figure 1a. Then, an observer sees radiation coming from short segments (“patches”) of the electron's trajectory which are nearly parallel to the line of sight (very much like for pure synchrotron radiation). The magnetic field in every patch is almost uniform but it varies from patch to patch. The radiation is pulsed with a typical duration $\tau_p \sim 1 / \omega_c$. The characteristic frequency of the observed radiation is thus $\omega \sim \omega_c$. Note that in the time- or ensemble-averaged spectrum, the instantaneous field, B_\perp , which enters ω_c , should

be appropriately averaged, $\bar{B} \simeq \sqrt{\langle B_\perp^2 \rangle}$. In this case the emergent radiation is completely identical to synchrotron radiation from large-scale weakly inhomogeneous magnetic fields.

Second, $\delta \sim \alpha / \Delta\theta \ll 1$, i.e., the deflection angle is smaller than the beaming angle, so that the entire electron's trajectory is seen by an observer, as shown in Figure 1b. The particle moves along the line of sight almost straight and experiences high-frequency jittering in the perpendicular direction due to the random Lorentz force. We therefore refer the emerging radiation to as “jitter” radiation. Its spectrum is determined by random accelerations of the particle. Let's imagine an electron moving ultrarelativistically along the line of sight with a constant velocity, the transverse accelerations of the electron are small. In the laboratory frame, the electron passes through the magnetic field inhomogeneities having a typical scale $\lambda_B \sim k_B^{-1}$ with the velocity c . In the particle's frame (i.e., where its parallel velocity vanishes), the field correlation scale is $\lambda'_B \sim \lambda_B / \gamma \sim (k_B \gamma)^{-1}$ due to the Lorentz transformation. The electron's perpendicular acceleration changes significantly during $\tau \sim \lambda'_B / c \sim (\gamma k_B c)^{-1}$, so that the characteristic frequency of the emitted radiation is $\omega_{j0} \sim \tau^{-1} \sim \gamma k_B c$. In the laboratory frame, this frequency is boosted to $\omega_j = \gamma \omega_{j0}$. Thus, the spectrum of the emergent radiation is peaked at the frequency $\omega_j \sim \gamma^2 k_B c$. This frequency is higher than the critical synchrotron frequency in the uniform magnetic field of the same strength, ω_{c*} , namely

$$\frac{\omega_{c*}}{\omega_j} \simeq \frac{3}{2} \delta \ll 1, \quad (3)$$

as follows from equation (2).

We should warn here that despite apparent similarity of the jitter and free electron laser emission mechanisms, they are quite different. The wiggler field in free electron lasers is appropriately adjusted for the electron motion to be in phase with the produced radiation field to emit coherent radiation. Jitter radiation is, in general, incoherent.

3. THE STRUCTURE OF THE MAGNETIC FIELD IN GRB SHOCKS

To proceed further, a model for a magnetic field in GRB shocks is required. We use the only presently available quantitative theory of the magnetic field generation in shocks proposed by Medvedev & Loeb (1999). To be specific, we focus on internal shocks which produce γ -ray emission. External shocks which are responsible for the delayed afterglows may be treated similarly and will be considered in a future publication.

Shock fronts are shown to be natural sites of the magnetic field generation. Right before a shock, the inflowing (in the shock frame) bulk plasma particles meet the outflowing particles which were reflected (scattered) from the shock. Such a two-stream motion is kinetically unstable. The emergent magnetic field is random with zero mean and lies in the plane of the shock front, — perpendicular to the shock velocity. In principle, all plasma species participate in the instability. We assume the protons and electrons to be the only species and discuss their contributions separately.

It is important to emphasize that the generated magnetic field fills the entire volume of a shock shell and is not

located within a thin layer of order several skin depths near the front. There is a gas flow through a shock. Because of flux freezing the generated magnetic field is transported with the shocked material downstream. This material is replenished with a fresh one where a new magnetic field is thus continuously produced. Since the magnetic field is long-lived and does not decay in a dynamical time, as indicated by numerical simulations (see references in Medvedev & Loeb 1999), this field will be present in the entire ejecta.

3.1. Fields produced by the electrons and protons

In this subsection we briefly remind main results of the theory of Medvedev & Loeb (1999) for future reference. Since electrons are light, the instability induced by them is rapid: the typical e -folding length (i.e., the e -folding time times the shock speed) is much smaller than the characteristic shock thickness determined by the Larmor radius of heavier protons. Therefore, the magnetic field energy grows rapidly and reaches the approximate equipartition with the electron kinetic energy,

$$\frac{\bar{B}_e^2}{8\pi} = \eta_e \gamma_{\text{int}} m_e c^2 n = \frac{m_e}{m_p} e_t \eta_e, \quad (4)$$

i.e., $\epsilon_{Be} = \bar{B}_e^2/8\pi e_t = (m_e/m_p)\eta_e$, where η_e is the efficiency factor for the electrons which incorporates uncertainties due to the nonlinear phase of the instability, one infers from numerical simulations that generically $\eta_e \simeq 0.1-0.01$, γ_{int} is the relative Lorentz factor of two colliding shells which produce an internal shock, $\gamma_{\text{int}} \sim 2-4$, and n is the number density of particles in the expanding shell, before the shock. The spatial correlation scale, k_{Be} , of the field behind the shock is

$$k_{Be} = \frac{4\gamma_{\text{int}}\omega_{pe}}{2^{1/4}\bar{\gamma}_e^{1/2}c}, \quad (5)$$

where $\omega_{pe}^2 = 4\pi e^2 n/m_e$ is the electron plasma frequency squared, $\bar{\gamma}_e$ is the initial effective thermal Lorentz factor of the streaming electrons, and an extra factor of $4\gamma_{\text{int}}$ is due to the relativistic shock compression.

The protons may generate magnetic fields too. Since they are much heavier than electrons, the spatial coherence length and the e -folding length are comparable to the thickness of the collisionless shock. Therefore, the field does not have enough time to grow during the flow transit through the shock. It may however grow behind the shock if the two-stream motion of the protons persists there. If this is the case, then there are two possibilities. First, if there is no energy transfer from the protons to the electrons or if it is slow compared to the rate of the field growth, then the magnetic field energy may be as large as

$$\frac{\bar{B}_p^2}{8\pi} = \eta_p \gamma_{\text{int}} m_p c^2 n = e_t \eta_p \sim 0.1 e_t, \quad (6)$$

provided $\eta_p \sim 0.1$. Second, if the energy transfer is fast, which may be the case in fields which are in equipartition with the electrons or stronger, then the protons may efficiently damp their energy into the emitting electrons,

²Note, the inflowing electrons are cold; they are not Fermi accelerated yet. Note also that $\bar{\gamma}_e$ cannot be greater than γ_{int} for the instability to operate. Otherwise, no magnetic field is produced.

so that the resultant field will be $\bar{B}_p^2/8\pi \sim \bar{B}_e^2/8\pi$. Alternatively, if no magnetic field is generated downstream the shock, the strength of the field produced by the protons may be orders of magnitude lower. Which case realizes may be learned from numerical particle simulations or from observations. We keep $\epsilon_{Bp} = \bar{B}_p^2/8\pi e_t$ as a parameter. The characteristic correlation scale of the generated magnetic field is

$$k_{Bp} = \frac{\omega_{pp}}{2^{1/4}\bar{\gamma}_p^{1/2}c}, \quad (7)$$

where $\omega_{pp}^2 = 4\pi e^2 n/m_p$, $\bar{\gamma}_p \sim 2$ is the initial effective thermal Lorentz factor of the streaming protons. The compression factor, $4\gamma_{\text{int}}$, is absent because the field is likely produced after the compression occurs.

3.2. The model

From equations (2), (4), and (5), we estimate the δ -parameter for the electrons,

$$\delta_e = \frac{1}{2^{7/4}} \left(\frac{\bar{\gamma}_e}{\gamma_{\text{int}}} \right)^{1/2} \sqrt{\eta_e} \equiv \phi \sqrt{\eta_e} \lesssim 1. \quad (8)$$

The exact value of $\phi = 2^{-7/4}(\bar{\gamma}_e/\gamma_{\text{int}})^{1/2}$ is somewhat uncertain: $\bar{\gamma}_e$ may evolve during the instability from its initial value $\bar{\gamma}_e \sim 2-3$ to $\bar{\gamma}_e \sim \gamma_{\text{int}} \sim 3-4$ due to nonlinear effects.² The numerical prefactor may also be affected. Therefore we assume that possible values of δ_e are in the range $1 \lesssim \delta_e \lesssim 10^{-2}$ (given the uncertainty in η_e from 0.1 to 0.01) and generically $\delta_e \sim 0.1$. The δ -parameter for the protons is

$$\delta_p = 2^{-1/4} (\bar{\gamma}_p \gamma_{\text{int}})^{1/2} \frac{m_p}{m_e} \sqrt{\eta_p} \gg 1, \quad (9)$$

unless η_p is too small: $\eta_p \lesssim 10^{-7}$ (i.e., $\epsilon_{Bp} \lesssim 10^{-3}\epsilon_{Be}$).

As will be shown below in §4, a spatial spectrum of the magnetic field \bar{B}_e with $\delta_e < 1$ is required to calculate the spectrum of jitter radiation. This distribution of \bar{B}_e over scales is difficult to find from the first principles because it is determined by fully nonlinear dynamics of the instability process. Some constraints may however be drawn. First, the two-stream instability produces magnetic fields in a finite range of scales, $0 \leq k \leq k_{\text{crit},e}$, where $k_{\text{crit},e} \sim k_{Be}$ to within a numerical factor of order unity. Second, the field grows until it becomes strong enough to deflect the particles in the transverse direction by ~ 1 radian on a scale of the field coherence length, i.e., $\bar{B}_e^{-1} \propto \rho_e \sim k_{Be}^{-1}$. If we now assume that each Fourier harmonic, B_k , is amplified independently of others, we obtain: $B_k \propto k$ for $k \leq k_{\text{crit},e}$. This is the lower limit: the spectrum of the magnetic field can only be steeper than linear.

In reality, all Fourier harmonics are coupled. Thus, when at least one harmonic reaches the sub-equipartition strength, the streaming electrons are isotropized by random Lorentz forces. This prevents the growth of other harmonics. Therefore, the spectrum of the field will be steeper than linear and will have a maximum near k_{Be} . The simplest possible model is a power-law,

$$B_k = \begin{cases} C_B k^\mu, & \text{if } 0 \leq k \leq k_{Be}, \\ 0, & \text{otherwise,} \end{cases} \quad (10)$$

where C_B is a normalization constant and $\mu \geq 1$ is a power-law spectral index of the magnetic field being a free parameter here. The constant C_B may be determined using Parseval's theorem,³ $\lim_{L \rightarrow \infty} \int_{-L/2}^{L/2} B_e^2 dx = \frac{1}{\pi} \int_0^\infty B_k^2 dk$, where L is the system size. Taking into account that $\int B_e^2 dx = \bar{B}_e^2 L = \bar{B}_e^2 cT$, where T is the total duration of the pulse, we write

$$C_B^2 = \pi (2\mu + 1) cT \bar{B}_e^2 k_{Be}^{-(2\mu+1)}. \quad (11)$$

The magnitude of the field, \bar{B}_e , is given by equation (4).

Strictly speaking, this model may be used for not too small k 's: $k > k_{\min}$, where k_{\min} is set by the condition: $\gamma/(\rho_e k_{\min}) = 1$, see equation (2). The field harmonics with $k < k_{\min}$ are large-scale ones and they contribute to synchrotron radiation. Using equation (2), it is easy to obtain that $k_{\min} = \delta_e k_{Be}$. It is also useful to introduce the small-scale field component as follows,

$$\bar{B}_{SS}^2 = \int_{k_{\min}}^{k_{Be}} B_k^2 dk, \quad \frac{\bar{B}_{SS}^2}{\bar{B}_e^2} = 1 - \delta^{2\mu+1}. \quad (12)$$

Hereafter, we omit the subscripts by δ ; this should not cause any confusion.

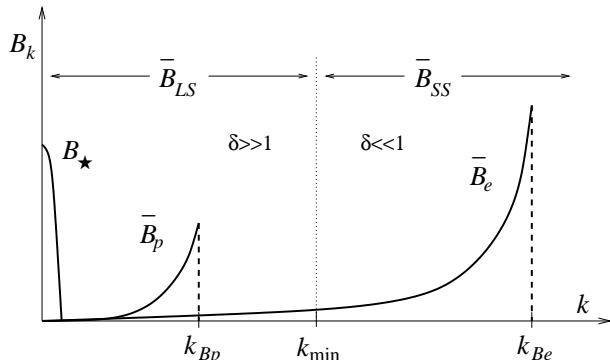


FIG. 2.— The model for the magnetic field in GRB shocks.

To summarize, we assume the following structure of the magnetic field sketched in Figure 2. First, there is a magnetic field produced by the electrons, \bar{B}_e , the magnitude of which is given by equation (4). A large fraction of this field contributes to the small-scale component, in accordance with equation (12). Its distribution over spatial scales is described by a power-law with the index μ , see equation (10). The rest, $\bar{B}_e^2 - \bar{B}_{SS}^2$, contributes to the large-scale component. Second, there is a magnetic field produced by the protons, \bar{B}_p . This field is a large-scale field. Both \bar{B}_e and \bar{B}_p are random with zero mean. Third, there could be an ordered magnetic field left from a magnetized progenitor, B_\star . We define the total large-scale magnetic field as follows,

$$\bar{B}_{LS}^2 = \bar{B}_0^2 + (\bar{B}_e^2 - \bar{B}_{SS}^2), \quad \bar{B}_0^2 = B_\star^2 + \bar{B}_p^2, \quad (13)$$

where \bar{B}_0 is the fraction of the large-scale field which is not produced by the electrons.

³We use the following definition of the Fourier transform: $f(\omega) = \int f(t)e^{-i\omega t} dt$.

⁴Physically, a particle moves along a helical trajectory about field lines of a large-scale field. This trajectory is slightly perturbed by high frequency jittering in the (instantaneous) transverse direction due to a small-scale field component. The intensities of the spectral sub-components are determined by the magnetic field energy densities at large and small scales.

4. RADIATION FROM SMALL-SCALE FIELDS: QUANTITATIVE THEORY

In §2 we qualitatively demonstrated that there are two regimes of radiation. An ultrarelativistic electron propagating through small-scale fields generated only by the electrons ($\delta \ll 1$) emits jitter radiation. The electron moving through larger-scale fields generated only by the protons ($\delta \gg 1$) emits synchrotron radiation. The radiation spectrum from a magnetic field with a broadband distribution over scales is neither of the above and must be calculated by appropriate scale averaging of a particle trajectory. However, for a bimodal field distribution of §3.2 such that the magnetic energy in B_k harmonics for which $\delta \sim 1$ (i.e., where the transition from a jitter to synchrotron regime occurs) is small, the separation of scales is possible. The resultant radiation will approximately be a composition of the jitter and synchrotron spectra.⁴ For clarity and illustration purposes, we derive the radiation properties and spectra in both limits separately. A rigorous treatment of a general case will be given elsewhere. All calculations in this section are done in the reference frame of the shocked material, unless stated otherwise.

4.1. Jitter radiation, $\delta \ll 1$

For sufficiently small δ 's such that $\alpha \ll \Delta\theta$, the velocity \mathbf{v} of a particle is almost constant whereas its acceleration $\mathbf{w} \equiv \dot{\mathbf{v}}$ varies with time. Calculating the Fourier component of the electric field using the Liénard-Wiechart (retarded) potentials, one arrives at the following expression for the total energy emitted per unit solid angle $d\Omega$ per unit frequency $d\omega$ (Landau & Lifshits 1975, §77; see also Rybicki & Lightman 1979, §3.2):

$$dW = \frac{e^2}{2\pi c^3} \left(\frac{\omega}{\omega'}\right)^4 \left| \mathbf{n} \times \left[\left(\mathbf{n} - \frac{\mathbf{v}}{c} \right) \times \mathbf{w}_{\omega'} \right] \right|^2 d\Omega \frac{d\omega}{2\pi}, \quad (14)$$

where $\mathbf{w}_{\omega'} = \int \mathbf{w} e^{i\omega' t} dt$ is the Fourier component of the particle's acceleration, $\omega' = \omega(1 - \mathbf{n} \cdot \mathbf{v}/c)$, and \mathbf{n} is the unit vector pointing towards the observer.

First, we can simplify the vector expression in (14). Indeed, in the ultrarelativistic case, the longitudinal component of the acceleration is small compared to the transverse component, $w_{\parallel}/w_{\perp} \sim 1/\gamma^2 \ll 1$. Therefore \mathbf{v} and \mathbf{w} are approximately perpendicular to each other. Second, the dominant contribution to the integral over $d\Omega$ comes from small angles $\theta \sim 1/\gamma$ with respect to the particle's velocity. Therefore, we approximately write $\omega' \simeq \omega(1 - v/c + \theta^2/2) \simeq \frac{1}{2}\omega(1 - v^2/c^2 + \theta^2) = \frac{1}{2}\omega(\theta^2 + \gamma^{-2})$. We now can replace integration over the solid angle $d\Omega \simeq \theta d\theta d\phi$ with integration over $d\phi d\omega'/\omega$ and integrate equation (14) over the azimuthal angle, ϕ , from 0 to 2π . The spectral energy finally becomes

$$\frac{dW}{d\omega} = \frac{e^2 \omega}{2\pi c^3} \int_{\omega/2\gamma^2}^{\infty} \frac{|\mathbf{w}_{\omega'}|^2}{\omega'^2} \left(1 - \frac{\omega}{\omega' \gamma^2} + \frac{\omega^2}{2\omega'^2 \gamma^4} \right) d\omega'. \quad (15)$$

The leading term in the above equation is due to high-frequency “jittering” of the electron as it moves through the random magnetic field. The second and third terms in the brackets are corrections due to the angular structure of the radiation field convolved with the relativistic beaming.

The acceleration \mathbf{w} is found from the equation of motion, $\dot{\mathbf{p}} = (e/c)\mathbf{v} \times \mathbf{B}$. In general, \mathbf{B} may vary both in amplitude and in direction. In relativistic GRB shocks, radiation is beamed; only a conical section bound by the opening angle $\theta_b \sim 1/\gamma_{\text{sh}}$ is seen by an observer, where γ_{sh} is the bulk Lorentz factor of the expanding shell. At a particular observing time, most of the radiation is coming from the brightened limb (Sari 1998; Panaitescu & Mészáros 1998). Because of relativistic aberration (Rybicki & Lightman 1979), the shock front is seen almost edge-on at the limb. On the other hand, the magnetic fields in the shock shell are random but always lie in the plane of the shock front (Medvedev & Loeb 1999). Choosing a coordinate system with \hat{x} -direction pointing towards the observer (in the shock frame) and \hat{x} - \hat{y} -plane being the shock front plane at the limb, we have $\mathbf{v} = c\hat{x}$, $\mathbf{B}_\perp = B_y\hat{y}$, and $\dot{\mathbf{p}} \simeq \gamma m_e w \hat{z}$. Then, the Fourier component of w is

$$w_{\omega'} = \frac{eB_{\omega'}}{\gamma m_e} = \frac{eB_{k'}}{\gamma m_e c}. \quad (16)$$

For the magnetic field distribution, we use the model (10).

At last, the spectral power $P(\omega) \equiv dW/dt d\omega$ (i.e., the energy emitted per unit time per unit frequency interval, measured in ergs $\text{s}^{-1} \text{Hz}^{-1}$) is obtained dividing the energy spectrum $dW/d\omega$ by the pulse duration, T (Rybicki & Lightman 1979). Combining equations (16), (10), (11) together and substituting into (15), we obtain

$$P(\omega) = r_e^2 c \gamma^2 \frac{\bar{B}_{SS}^2}{2\omega_j} J\left(\frac{\omega}{\omega_j}\right), \quad (17)$$

where $\omega/\omega_j \leq 2$, and $r_e = e^2/m_e c^2$ is the classical electron radius. As is expected, the characteristic frequency of the emergent radiation is

$$\omega_j = \gamma^2 k_B c = 2^{7/4} \gamma^2 \gamma_{\text{int}} \bar{\gamma}_e^{-1/2} \omega_{pe}, \quad (18)$$

cf., equations (5) and (8). The function J is defined as

$$J(\xi) = (2\mu + 1)\xi^{2\mu} \left[I\left(\min\left[2; \frac{\xi}{\delta}\right]\right) - I(\xi) \right], \quad (19)$$

where I is the integral,⁵ $I(\xi) = \int \xi^{-2\mu} (1 - \xi + \frac{1}{2}\xi^2) d\xi$, and $\min[a; b]$ denotes the smallest of a and b . From equations (2), (4), (18), we have $\omega_j = \gamma^2 \bar{B}_e / \delta m_e c$. Equation (17) may now be cast into the form,

$$P(\omega) = \frac{e^2}{2c} \delta^2 \frac{\omega_j}{\gamma^2} \frac{\bar{B}_{SS}^2}{B_e^2} J\left(\frac{\omega}{\omega_j}\right). \quad (20)$$

This spectrum is shown in Figure 3 for several values of μ . In general, the steeper the field distribution, $B_k \propto k^\mu$,

⁵We keep this integral in a general form because it contains logarithmic terms for $\mu = 0.5, 1, 1.5$.

⁶Small-scale magnetic fields present in the shock provide effective collisions in the otherwise collisionless plasma and make the Fermi acceleration to operate (Medvedev & Loeb 1999).

⁷Recent studies indicate that the high-frequency spectral power index in the prompt GRBs is ~ -1 which translates to $p \sim 3$. We keep $p = 2.5$ for illustrative purposes.

the more peaked is the radiation spectrum and the closer the peak frequency to $2\omega_j$. Note, the discontinuity of the slope is artificial. This is due to the k_{min} -cutoff because the model we use does not continuously interpolate between the jitter and synchrotron radiation limits (i.e., between $\delta \ll 1$ and $\delta \gg 1$ cases). This discontinuity is less prominent for large μ 's and small δ 's.

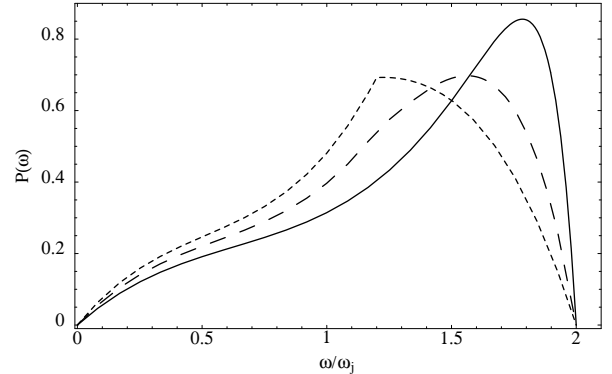


FIG. 3.— The arbitrarily normalized power spectra, $P(\omega)$, of jitter radiation (linear-linear plot) emitted by a single electron for several values of the magnetic field spectral index, $\mu = 1$ (dotted), $\mu = 3$ (dashed), and $\mu = 10$ (solid). Here $\delta = 0.6$ and we keep the value of the small-scale magnetic field fixed, $\bar{B}_{SS}^2/8\pi = \bar{B}_e^2/8\pi$.

The total emitted power may be obtained by integrating (17) over frequencies. A simpler way is to express it in terms of electron’s acceleration, i.e., $dW/dt = (2e^2\gamma^4/3c^3)(w_\perp^2 + \gamma^2 w_\parallel^2)$ (Rybicki & Lightman 1979) and substitute $w_\parallel = 0$ and w_\perp given by (16). The result is

$$dW/dt = (2/3)r_e^2 c \gamma^2 \bar{B}_{SS}^2. \quad (21)$$

Note, this expression is identical to that for a synchrotron radiation in which a uniform field, B_\perp^2 , is replaced with its average, $\bar{B}_{SS}^2 = \langle B_\perp^2 \rangle$.

We are now able to calculate the jitter radiation spectrum from an ensemble of electrons. We assume that electrons are accelerated in the shock⁶ to a power-law distribution $N(\gamma) = C_N \gamma^{-p}$ (where C_N is a normalization constant) with a minimum Lorentz factor, i.e., $\gamma_{\text{min}} \leq \gamma < \infty$. The index p must be $p \geq 2$ so that energy does not diverge at large γ 's. We assume the standard value,⁷ $p = 2.5$ (Sari, Narayan, & Piran 1996), unless stated otherwise. The spectrum is found from

$$P_{\text{ens}}(\omega) = \int_{\gamma_{\text{min}}}^{\infty} N(\gamma) P(\omega) d\gamma, \quad (22)$$

noting that $\omega_j \equiv \omega_j(\gamma) \propto \gamma^2$, i.e., in exact analogy with synchrotron radiation, $\omega_c \propto \gamma^2$. We obtain

$$P_{\text{ens}}(\omega) = \frac{C_N}{2\gamma_{\text{min}}^{p-1}} \left(\frac{\omega}{\omega_{jm}}\right)^{-\frac{p-1}{2}} \int_0^{\omega/\omega_{jm}} \xi^{(p-1)/2} P(\xi) d\xi, \quad (23)$$

where we introduced the characteristic frequency of radiation $\omega_{jm} \equiv \omega_j(\gamma_{\min})$, cf. equation (18),

$$\omega_{jm} = 2^{7/4} \gamma_{\min}^2 \gamma_{\text{int}} \bar{\gamma}_e^{-1/2} \omega_{pe}, \quad (24)$$

At low and high frequencies, the spectra may be obtained analytically as follows,

$$P_{\text{ens}}(\omega) \propto \begin{cases} \left(\frac{\omega}{\omega_{jm}}\right)^1, & \omega \ll \omega_{jm}, \\ \left(\frac{\omega}{\omega_{jm}}\right)^{-(p-1)/2}, & \omega \gtrsim \omega_{jm}, \end{cases} \quad (25)$$

At high frequencies, the spectrum is analogous to the synchrotron case. The electron power-law index determines the slope. At low frequencies, the spectrum is linear in frequency, in contrast to the synchrotron spectrum which is softer and scales as $P_{\text{syn}}(\omega) \propto \omega^{1/3}$. The spectrum of radiation from single-speed electrons is peaked at $\omega \simeq 2\omega_j$ for large μ 's, i.e., for a peaked magnetic field distribution, as discussed above (see also Figure 3). Therefore, the spectral break due to the γ_{\min} -cutoff occurs at

$$\begin{aligned} \nu_{j,\text{break}} &\simeq 2\omega_{jm}/2\pi = (2^{7/4}/\pi) \gamma_{\min}^2 \gamma_{\text{int}} \bar{\gamma}_e^{-1/2} \omega_{pe} \\ &\simeq 6.0 \times 10^9 \gamma_{\min}^2 \gamma_{\text{int}} \bar{\gamma}_e^{-1/2} n_{10}^{1/2} \text{ Hz}, \end{aligned} \quad (26)$$

where $n_{10} \equiv n/10^{10} \text{ cm}^{-3}$. The above frequency is calculated in the frame of the relativistic expanding shell. This frequency is boosted in observer's frame by a factor of γ_{sh} .

The model of jitter radiation contains two extra parameters, compared to the model of synchrotron radiation. These parameters are the deflection-to-beaming ratio, δ , and the magnetic field index, μ , which determines the peakedness of the magnetic field over spatial scales. We now investigate how the spectrum of the emergent radiation depends on these parameters.

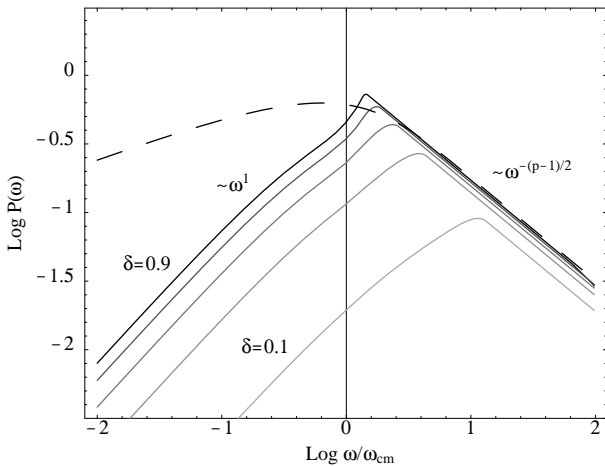


FIG. 4.— Spectral power $P(\omega)$ of radiation (log-log plot, arbitrary units) emitted by the power-law distributed electrons vs. ω/ω_{cm} for $\delta = 0.9, 0.7, 0.5, 0.3, 0.1$ (from top to bottom). Here $\mu = 1$ and $p = 2.5$. The synchrotron spectrum with the same magnetic field strength is shown (dashed curve) for comparison. The value of $\bar{B}_{SS}^2/\bar{B}_e^2$ is kept fixed for all δ 's.

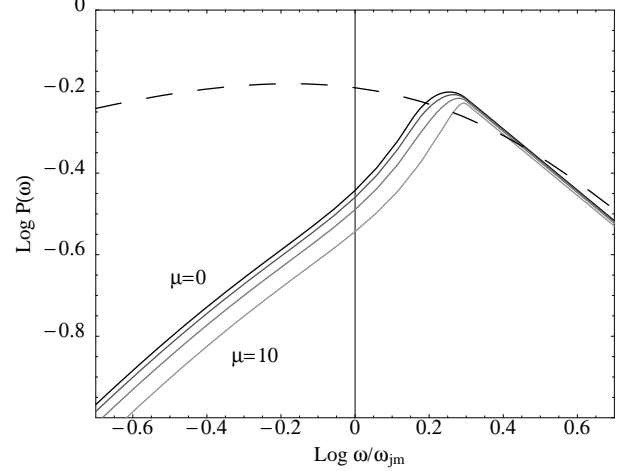


FIG. 5.— Spectral power $P(\omega)$ of radiation (log-log plot, arbitrary units) emitted by the power-law distributed electrons vs. ω/ω_{jm} for $\mu = 0, 1, 3, 10$ (from top to bottom). Here $\delta = 0.7$ and $p = 2.5$. The synchrotron spectrum with the same magnetic field strength is shown (dashed curve) for comparison. The value of $\bar{B}_{SS}^2/\bar{B}_e^2$ is kept fixed for all μ 's.

Figure 4 represents the spectral power, $P(\omega)$, given by equations (20), (23), as a function of ω/ω_{cm} , where $\omega_{cm} \equiv \omega_c(\gamma_{\min})$, for various values of δ . The dashed curve represents the synchrotron spectrum which corresponds to the same magnetic field strength. Note, the frequency is normalized by the synchrotron break frequency, ω_{cm} (not the jitter break frequency, ω_{jm}), to emphasize that, for the fixed field magnitude, \bar{B}_{SS}^2 , the jitter frequency increases with decreasing δ , in accordance with equation (3). One can see that jitter radiation is well described by a broken power-law given by equation (25). Notice also little change in the spectrum shape near the break frequency and the overall decrease of $P(\omega)$ as δ decreases.

Figure 5 shows $P(\omega)$ vs. ω/ω_{jm} for a few values of the magnetic field index, μ . In general, the ratio $\bar{B}_{SS}^2/\bar{B}_e^2$ depends on μ . To highlight the effect of the magnetic spectrum shape alone, we keep $\bar{B}_{SS}^2/\bar{B}_e^2$ fixed for all μ 's. One can see from Figure 5 that μ has little effect on the overall shape of the radiation spectrum. However, as one goes from a flat ($\mu = 0$) to a peaked ($\mu = 10$) magnetic field distribution, the change in slope at the break frequency becomes more abrupt.

4.2. Synchrotron radiation, $\delta \gg 1$

For completeness, we also consider the case of $\delta \gg 1$. In this case, $\alpha/\Delta\theta \gg 1$ while still $\lambda_B/\rho_L \ll 1$ for energetic electrons. The spectral power emitted by a single electron is given as (Landau & Lifshits 1975, §77 and §74)

$$\frac{dW}{dt d\omega} = \frac{e^2}{\sqrt{3}\pi c \gamma^2} \left\langle \tilde{\omega}_c F\left(\frac{\omega}{\tilde{\omega}_c}\right) \right\rangle, \quad (27)$$

where $\tilde{\omega}_c = \frac{3}{2}\gamma^2 e \tilde{B}_\perp / m_e c$, $\langle \dots \rangle$ denotes the average over the electron's trajectory, and "tilde" denotes the local (instantaneous) quantity. Here $F(\xi) = \xi \int_\xi^\infty K_{5/3}(\xi') d\xi'$ and $K_{5/3}(x)$ is the modified Bessel function of 5/3 order. As for the spectrum from a plasma, the observed radiation comes from regions with different field strength. Therefore, one has to replace \tilde{B}_\perp in (27) with the ensemble av-

erage, $\bar{B} = \sqrt{\langle \tilde{B}_\perp^2 \rangle}$, which rigorously yields the standard synchrotron spectrum.

5. JITTER+SYNCHROTRON MODEL OF GRB EMISSION

We now use the model of magnetic fields discussed in § 3.2 to construct a GRB spectral model. All calculations are performed in the frame of the expanding shell. The transition to observer's frame is obvious. The magnetic field in the shock shell was shown to be sub-divided into small-scale and large-scale components. The small-scale field, for which $\delta \lesssim 1$, yields jitter radiation. Its spectral power is given by equations (20), (23). The large-scale field, for which $\delta \gg 1$, yields synchrotron radiation. The relevant theory may be found in Rybicki & Lightman (1979). The composite spectrum, thus, contains both jitter and synchrotron components and may be schematically represented as follows,

$$P_{J+S}(\omega) = P_J(\omega; \bar{B}_{SS}, \delta, \mu) + P_S(\omega; \bar{B}_{LS}). \quad (28)$$

This approximation is valid for the field distribution from §3.2 unless $\delta \sim 1$, as discussed in the beginning of §4. It is convenient to normalize frequencies onto the jitter frequency, ω_{jm} , which is independent of the magnetic field strength, cf., equation (26). The synchrotron-to-jitter frequency ratio is then

$$\frac{\omega_{cm}}{\omega_{jm}} = \frac{\omega_c}{\omega_j} \simeq \frac{3 \bar{B}_{LS}}{2 \bar{B}_{SS}} \delta, \quad (29)$$

as follows from equations (3), (13).

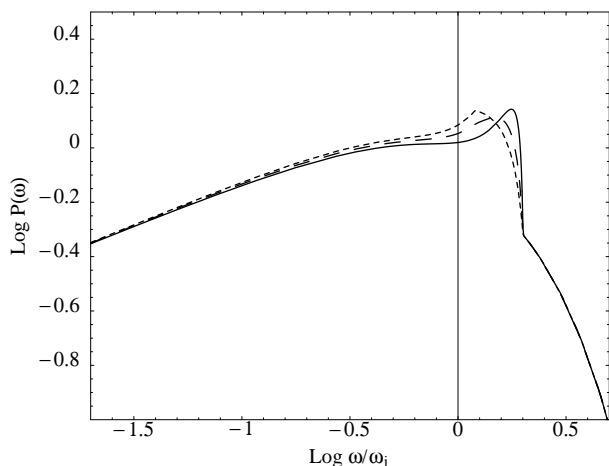


FIG. 6.— The arbitrarily normalized, composite power spectra, $P_{J+S}(\omega)$, (log-log plot) emitted by a single electron for several values of the magnetic field spectral index, $\mu = 1$ (dotted), $\mu = 3$ (dashed), and $\mu = 10$ (solid) for $\delta = 0.6$ and $\bar{B}_0^2/\bar{B}_{SS}^2 = 3$.

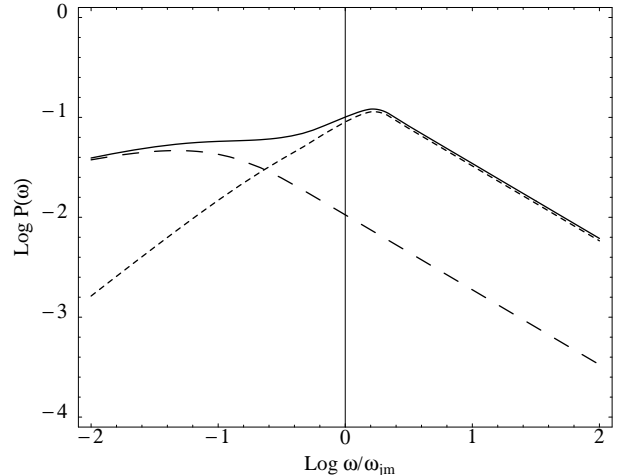


FIG. 7.— A typical composite power spectrum, $P_{J+S}(\omega)$, (log-log plot, arbitrary units) for the power-law distributed electrons with $p = 2.5$ for $\mu = 1$, $\delta = 0.3$, and $\bar{B}_0^2/\bar{B}_{SS}^2 = 0$ is shown. The synchrotron (long-dashed curve) and jitter (short-dashed curve) sub-components are also shown.

Figure 6 represents the spectrum emitted by single-speed electrons for the same values of μ as in Figure 3. One can clearly see a sharp feature on top of the broad synchrotron spectrum. Integrating this spectrum over the power-law distribution of γ 's, we obtain the composite “jitter+synchrotron” (JS) model of GRBs. A typical example is shown in Figure 7. In general, there are two bumps: the sharp one is near the jitter frequency and the other, broad bump, is associated with synchrotron emission. Depending on the ratio $\bar{B}_{LS}^2/\bar{B}_{SS}^2$, these bumps may overlap to produce either featureless broad or sharply peaked spectra, as well. The high-frequency tail always scales as $P_{J+S}(\omega) \propto \omega^{-(p-1)/2}$. The dependence of the spectrum from δ is displayed in Figure 8. As an example, we take $\bar{B}_0^2/8\pi = \bar{B}_{SS}^2/8\pi$ and $\mu = 10$ (for such μ 's $\bar{B}_{SS}^2/8\pi \simeq \bar{B}_e^2/8\pi$, and, therefore $\bar{B}_{LS}^2/8\pi \simeq \bar{B}_0^2/8\pi$). A sharp jitter feature is easily seen in the spectrum. As δ decreases, the synchrotron bump moves towards lower frequencies and decreases in amplitude. The jitter peak decreases even faster and the spectral feature becomes less prominent. The other parameter, μ , determines the ratio $\bar{B}_{LS}^2/\bar{B}_{SS}^2$ but, besides this, its effect onto the spectrum is weak (cf., Figure 5) and is, therefore, not shown.

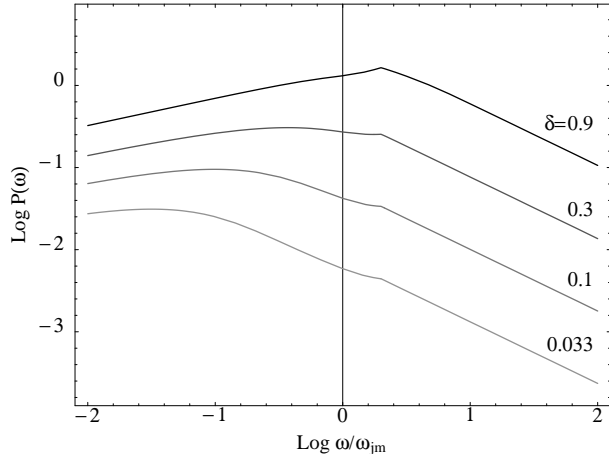


FIG. 8.— The composite power spectra, $P_{J+S}(\omega)$, (log-log plot, arbitrary units) for the power-law distributed electrons with $p = 2.5$ for $\delta = 0.9, 0.3, 0.1, 0.033$, $\bar{B}_0^2/\bar{B}_{SS}^2 = 1$ and $\mu = 10$.

The spectrum of radiation depends on the relative magnitudes of the large- and small-scale field components. Figure 9 represents spectra for $\mu = 10$ and various values of the ratio $\bar{B}_0^2/\bar{B}_{SS}^2 \approx \bar{B}_{LS}^2/\bar{B}_{SS}^2$. Figure 9a shows the spectral power vs. frequency. For strong large-scale fields, the synchrotron spectral component dominates. As $\bar{B}_{LS}^2/\bar{B}_{SS}^2$ decreases, the synchrotron peak moves towards lower frequencies. The amplitude of the synchrotron peak decreases too. The position and the amplitude of the jitter peak remain almost unchanged. Thus, in the limit $\bar{B}_{LS}^2/\bar{B}_{SS}^2 \rightarrow 0$, the spectrum becomes purely jitter. It is illustrative to depict the spectral flux, $F(\omega) \equiv P(\omega)/\omega$ [observationally, this quantity is proportional to the photon spectral flux, $N(E)$, measured in units: photons $\text{s}^{-1} \text{cm}^{-2} \text{keV}^{-1}$], as presented in Figure 9b. It is seen that the slope of the flux below the jitter break continuously decreases as $\bar{B}_{LS}^2/\bar{B}_{SS}^2$ decreases. The synchrotron asymptotic slope $\propto \omega^{-2/3}$ is shown for comparison. It is interesting that for $\bar{B}_{LS}^2/\bar{B}_{SS}^2 \lesssim 10^{-1}$ (the actual value depends on δ ; the larger δ , the larger the ratio), there is a portion in the spectrum which has the power-law index being less than $-2/3$ and approaching zero in the limit of the vanishing large-scale field. We discuss this property in §6 in the context of the “line of death” for synchrotron radiation in GRBs.

Finally, it is worthwhile to compare the peak spectral fluxes of jitter, $F_{J,\max} \equiv F_J(\omega_{jm})$, and synchrotron, $F_{S,\max} \equiv F_S(\omega_{cm})$, radiation,

$$\frac{F_{J,\max}}{F_{S,\max}} = f(p, \mu) \delta^2, \quad (30)$$

where $f(p, \mu)$ is a function of two power-law indices, p and μ . The above equation may be readily obtained from equations (23), (20), and, for instance, (27). For $\mu \gg 1$, the function f depends on μ only weakly while, given the spectrum, p is found by fitting the large frequency slope. Therefore, for a given spectrum with two sub-components, both significant parameters, namely $\bar{B}_{LS}^2/\bar{B}_{SS}^2$ and δ , are uniquely found from equations (29) and (30).

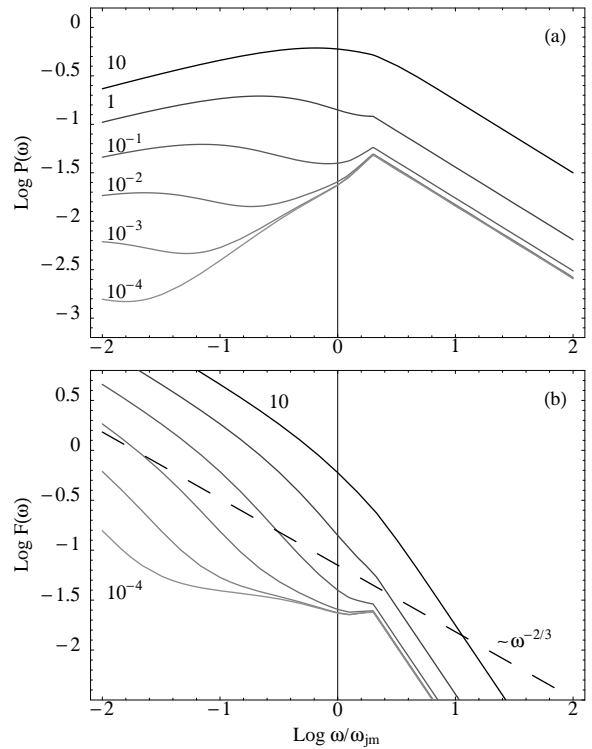


FIG. 9.— The composite spectra (log-log plots, arbitrary units) for the power-law distributed electrons with $p = 2.5$ for $\bar{B}_0^2/\bar{B}_{SS}^2 = 10 - 10^{-4}$, $\delta = 0.2$, and $\mu = 10$. (a) — Spectral power $P_{J+S}(\omega)$; (b) — Spectral flux $F_{J+S}(\omega) \equiv P_{J+S}(\omega)/\omega$.

6. COMPARISON WITH OBSERVATIONS

In §5 we constructed a composite, jitter+synchrotron model of radiation emitted from internal shocks of GRBs, assuming that the magnetic fields are produced in these shocks via the relativistic two-stream instability (Medvedev & Loeb 1999). Several observational predictions can now be drawn. We compare them with presently available observational data. For future reference, we define the photon spectral index, s , as follows,

$$F(\omega) \propto \omega^s. \quad (31)$$

Here we remind that $F(\omega) \equiv P(\omega)/\omega \propto N(E)$, where $N(E)$ is the number of observed photons per unit time, per unit energy range, per unit area.

We have shown that prompt GRB spectra consist of two spectral sub-components, namely synchrotron and jitter. The synchrotron component is, as usual, well approximated by the smoothly broken power-law, also referred to as the Band function (Band et al. 1993) or the GRB function. The jitter component is better approximated by a sharply broken power-law with the hard and soft photon indexes being equal to $s = -(p+1)/2$ and $s = 0$ respectively. The position of the jitter peak is independent of the magnetic field strength, in contrast to the synchrotron peak, but depends on the particle (electron) density in the relativistic expanding shell, see equation (26).

6.1. Low-frequency spectra and the “Line of Death”

The optically thin synchrotron model of GRBs makes a solid prediction. Namely, the soft photon spectral index must be in the range $-3/2 \leq s \leq -2/3$, depending on the strength of the magnetic field if strong synchrotron cooling of the emitting electrons in the fireball is taken into account (Katz 1994; Sari, Narayan, & Piran 1996). Thus, the photon index in this model can never be greater than $-2/3$, creating a testable “line of death” for the synchrotron shock model (Katz 1994). There is, however, a growing observational evidence that many bursts violate this prediction (Crider et al. 1997; Strohmayer et al. 1998; Preece et al. 1998; Frontera et al. 1999). For instance, Preece et al. (1998) have studied time-resolved spectra of the bursts collected by the LAD from the BATSE instrument. They found 23 out of 137 bursts which violate the optically thin synchrotron model. Frontera et al. (1999) demonstrated that about 50% of time-resolved spectra the bursts observed by the Wide Field Camera on board of the *BeppoSAX* before May 1998 also violate this model. The proposed explanations, which include Compton up-scattering of low-energy photons (Liang et al. 1997), synchrotron self-absorption (Papathanassiou 1999), and the influence of the pair annihilation in the fireball photosphere (Eichler & Levinson 1999), though possible, seem rather *ad hoc* and suffer from drawbacks. The Compton up-scattering model strictly requires a single up-scattering event per photon which requires the column density to self-adjust to a few g/cm^2 . The self-absorption model results in large optical depths and, thus, weak emitted flux and very low radiation efficiency. The photospheric model requires an extremely low baryonic load. For more discussion see Mészáros (1999).

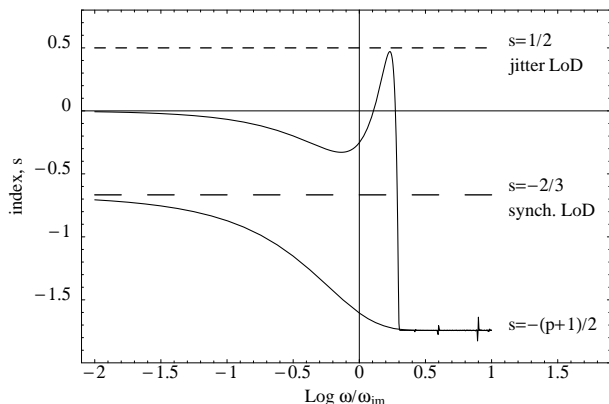


FIG. 10.— The power-law index, s , vs. $\log(\omega/\omega_{jm})$ for synchrotron and jitter radiation with $\mu = 10$, $\delta = 0.2$, $\bar{B}_{LS}^2/\bar{B}_{SS}^2 = 1$. The synchrotron and jitter “lines of death” (LoD) are shown.

The JS model provides a natural resolution of this puzzle. Figure 10 represents the photon index as a function of a logarithm of frequency for the synchrotron and jitter cases⁸. When jitter radiation dominates, the low-energy photon index tends towards its asymptotic value of $s = 0$, thus shifting the “line of death” to harder spectra. In principle, the indexes as large as $s = 1/2$ are allowed by our model. Positive s , however, are quite unlikely. These predictions are in good agreement with observational data. Namely, only two bursts out of those studied by Preece

et al. (1998) are above the $s = 0$ line by more than 1σ and all bursts studied by Frontera et al. (1999) except the peculiar one, GRB 970111, fall below this line. At last, these three bursts are still consistent with $s = 1/2$ within statistical uncertainties.

6.2. Sharply broken power-law spectra of GRBs

Most of the observed bursts are well-fitted by the GRB function (Band et al. 1993). However, there are bursts with a sharp curvature of the spectrum at the break energy. For such bursts a broken power-law model generates better χ^2 fits than the GRB function (see, e.g., Preece et al. 1998). In terms of the JS model, there are two cases in which such spectra occur. They can be observationally distinguished by the value of the soft (i.e., low-energy) photon index. First, it is the case of purely jitter radiation: $\bar{B}_{LS}^2/\bar{B}_{SS}^2 \rightarrow 0$ and there is no synchrotron peak (or this peak is too weak and is at low energies, outside the detector range), see Figure 9. These spectra are flat, $s \sim 0$, at low energies. Second, for large $\delta \sim 1$ and the equipartition between the large- and small-scale fields, $\bar{B}_{LS}^2/\bar{B}_{SS}^2 \sim 1$, similar spectral shapes are also obtained, see Figure 8. In this case, the soft photon index is $s \sim -2/3$, or it is in the range $-3/2 \leq s \leq -2/3$ if synchrotron cooling of the electrons is taken into account (Sari, Narayan, & Piran 1996). Thus, we expect fewer broken power-law bursts which have the soft photon indexes in the range $-2/3 \lesssim s \lesssim 0$. Figure 2 of Preece et al. (1998) indeed reveals a gap between the power-law bursts with $s \sim 0$ and $s \lesssim -2/3$. However, a larger number of such bursts is required to draw a statistically significant conclusion. We also should point out that if no ordered field is present in the ejecta, then $\bar{B}_{LS} \sim \bar{B}_{SS}$ is equivalent to $\bar{B}_p^2/8\pi \sim \bar{B}_e^2/8\pi$. This, in turn, naturally implies strong energy coupling and rough equipartition between the protons and the electrons, as discussed in §3.1.

6.3. Two-component spectral structure of GRB emission

The analysis done by Pendleton et al. (1994) of the bursts from the first BATSE catalog collected by the Large Area Detector (LAD) demonstrates that there is a large number of bursts which have the high-energy photon indexes (50 – 300 keV range) being much larger than the low-energy ones (20 – 100 keV range). No such behavior is observed at other energy ranges. Thus, this result may indicate the presence of more than one spectral component in the energy range 40 – 100 keV. (The absence of similar behavior at higher energies seems to rule out the inverse-Compton origin of a second spectral component.) On the other hand, such spectra are completely consistent with the JS model. They generally correspond to the well-separated synchrotron and jitter peaks and are characterized by small δ 's, $\delta \lesssim 0.1$, and weak large-scale fields, $\bar{B}_{LS}^2/\bar{B}_{SS}^2 \lesssim 0.01$, as is clearly seen from Figure 9.

6.4. “Lines” in GRB spectra

Whether emission and/or absorption features, often referred to as lines, in GRB spectra are real remains an open question for a long time (see, e.g., Briggs 1999 and Ryde 1999 for discussion). These features have been observed, for instance, by the KONUS experiment, *Venera*

⁸Little spikes on the lower curve are numerical artifacts.

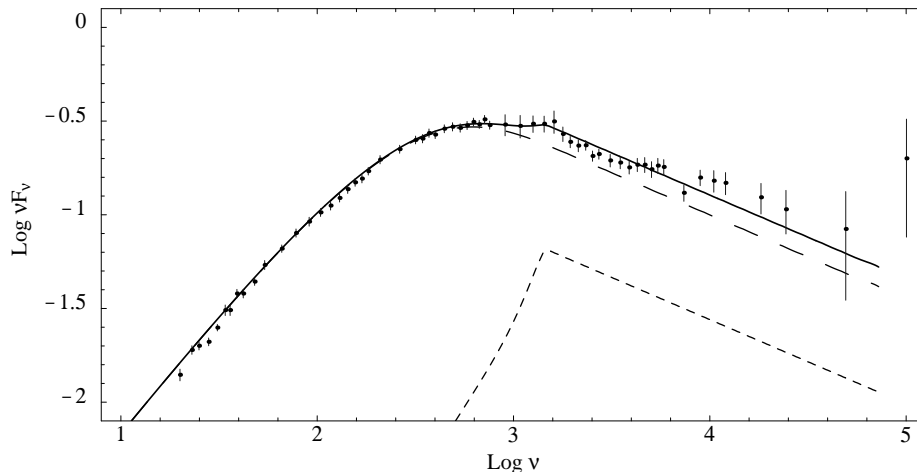


FIG. 11.— A visual fit of a spectral shape for GRB 910503. The inferred values are: $\bar{B}_0^2/\bar{B}_{SS}^2 = 7$, $\delta = 0.07$, $\mu = 10$, $p = 3.9$. The synchrotron (long-dashed curve) and jitter (short-dashed curve) spectral sub-components are also shown.

mission (Mazets et al. 1981) and by *Ginga* (Murakami et al. 1988). At that time, it was widely believed that these features are cyclotron lines due to a highly magnetized progenitor. The BATSE Spectroscopy Detectors (SD) refined these results. Palmer et al. (1994) studied almost two hundred bursts detected by SDs. No convincing line features were found. In a more recent analysis by Briggs (1999) of more than a hundred bursts observed by SDs before May 31, 1996, about 10 highly significant line features have been found. These are low-energy (~ 50 keV) emission features. Clearly, this controversy requires further studies. However, it seems likely that if lines exist, they are rare.

Not too surprisingly, the two-component JS model is able to produce spectra with emission line-like features. These are not lines in a strict sense because at energies higher than the “line” peak, the spectrum has no curvature and falls down as a power-law with $s = -(p + 1)/2$. Few such spectra are seen in Figure 8. These spectra are obtained (i) for rather low values of δ ($\delta \lesssim 0.3$), otherwise the synchrotron and jitter peaks overlap, and (ii) for a narrow range of $\bar{B}_{LS}^2/\bar{B}_{SS}^2$ ($0.1 \lesssim \bar{B}_{LS}^2/\bar{B}_{SS}^2 \lesssim 1$), otherwise either the spectral components are too well separated if the value of this ratio is small, or the jitter peak is too weak and unobservable if the ratio is large. We thus conclude that the spectra with emission features are not very common. They require some parameter tuning and, therefore, must be rare. Moreover, inhomogeneities and highly variable conditions in the GRB shocks may smear out weak spectral features completely.

At last, we present an illustrative example. Figure 11 shows the spectrum of GRB 910503 obtained using all capability of *CGRO*’s four experiments (Schaefer et al. 1998). Here the energy flux $\nu F_\nu \propto E^2 N(E) \propto \omega P(\omega)$ in units of $(\text{photons cm}^{-2} \text{ s}^{-1} \text{ keV}^{-1}) \times (E/100 \text{ keV})^2$ is plotted vs. frequency in units of keV. A sharp second peak at ~ 2 MeV is clearly seen. The solid curve in the figure represents a visual (i.e., not χ^2) spectral shape fit using the JS model. Here we fit the separation of the two peaks and their relative amplitudes; we didn’t fit the absolute flux and position of the synchrotron spectral break which depend on the energetics of the fireball. Note that the in-

tensity of a second, high-frequency (jitter) component is low. The values inferred from this fit are the following: $\bar{B}_{LS}^2/\bar{B}_{SS}^2 = 7$, $\delta = 0.07$, $p = 3.9$, and we took $\mu = 10$. We calculate the efficiency of the magnetic field generation in the shock from equation (2) assuming $\phi = 1/4$ as a typical value. We obtain $\eta_e \simeq 0.08$. The total magnetic field energy is calculated as $\epsilon_B = \epsilon_{Be}(1 + \bar{B}_{LS}^2/\bar{B}_{SS}^2)$, where ϵ_{Be} is found from equation (4) and we used $\bar{B}_{SS} \simeq \bar{B}_e$ for large μ . We obtain $\epsilon_B \simeq 4 \times 10^{-4}$, which is in agreement with the conclusion drawn by Chiang & Dermer (1999) from a completely different analysis that the magnetic field in this burst is well below the equipartition, $\epsilon_B \lesssim 10^{-2}$. Their argument goes from the fact that the low-energy spectrum of this burst is consistent with $F(\omega) \propto \omega^{-2/3}$. Evidently, synchrotron losses are small and the emitting electrons do not form a cooled distribution, which otherwise would result in $F(\omega) \propto \omega^{-3/2}$. This is possible only for very small values of ϵ_B .

7. CONCLUSION

In this paper we have shown that radiation produced by relativistic electrons in magnetic fields may differ quite substantially from synchrotron. This radiation, referred here to as jitter radiation, is produced in the magnetic fields which are highly inhomogeneous on very small spatial scales. Such fields are likely to be present in GRB shocks. We developed a quantitative theory of jitter radiation. Jitter radiation has a different spectrum and its peak frequency is independent of the field strength. However, the total (i.e., frequency integrated) emitted power of jitter radiation depends on the field strength and is exactly identical to that of synchrotron radiation. We also constructed a composite, two-component jitter+synchrotron spectral model of the prompt GRB emission. Predictions of this model seem to be in excellent agreement with presently available data and, likely, resolve some puzzling spectral properties of the prompt γ -ray emission. All this, we think, strongly supports that (i) the proposed jitter radiation mechanism operates in astrophysical objects and (ii) the magnetic field is generated in shocks by the two-stream instability. We emphasize that a reliable identification/detection of the jitter spectral features will provide a direct evidence that the magnetic field in GRBs is due to

the two-stream instability, since we presently unaware of any other mechanism which is capable of producing the required small-scale, large-amplitude fields. In general, the detection of both spectral components in GRB spectra would be a powerful and precise tool to investigate the properties of cosmological fireballs.

It is important to emphasize that the phenomenon of jitter radiation is intrinsic not only to internal shocks. Similar conditions (i.e., strong, small-scale fields) are expected to occur in external shocks which produce delayed afterglows, as well as in more conventional supernova shocks and relativistic jets. More speculatively, the above mechanism could allow to study the magnetic and electric fields in reconnection regions (remember, reconnection occurs on the electron skin depth scales) and small-scale structure of magnetic turbulence and cascade (e.g., in the interstellar medium).

The theory presented in this paper is only a “first step”. It is incomplete in a sense that it does not include the effects of both ordered and large-scale random

magnetic fields in a self-consistent way and, hence, does not smoothly interpolate between the two extremes of synchrotron and jitter mechanisms. The synchrotron self-absorption has been omitted. The model also does not consider some related effects. For instance, it is likely that random electric fields (i.e., strong Langmuir turbulence) are present in the cosmological collisionless shocks. These fields will definitely affect the radiation spectrum via a similar mechanism. It is also unclear now whether particle’s motion is ergodic in random fields (i.e., whether a particle “samples” strong and weak fields statistically homogeneously), and what could be the effect of nonergodicity on the observed spectrum. All these issues will be addressed in future publications.

The author is grateful to Ramesh Narayan and Norm Murray for their interest in this work, various insightful comments, and useful discussions and to George Rybicki and Avi Loeb for discussions. This work has been supported by NSF grant PHY 9507695.

REFERENCES

- Band, D., et al. 1993, *ApJ*, 413, 281
 Briggs, M. S. 1999, *astro-ph/9910362*
 Chiang, J. & Dermer, C. D. 1999, *ApJ*, 512, 699
 Covino, S., et al. 1999, *A&A*, 348, L1
 Crider, A., Liang, E. P., Smith, I. A., Preece, R. D., Briggs, M. S., Pendleton, G. N., Paciesas, W. S., Band, D. L., & Matteson, J. L. 1997, *ApJ*, 479, L39
 Eichler, D. & Levinson, A. 1999, *ApJ*, submitted; *astro-ph/9903103*
 Frail, D. A., Waxman, E., & Kulkarni, S. R. 1999, *ApJ*, submitted; *astro-ph/9910319*
 Frontera, F., et al., 1999, *ApJS*, accepted; *astro-ph/9911228*
 Galama, T. J., et al. 1999, *Nature*, 398, 394
 Ghisellini, G. & Lazzati, D. 1999, *MNRAS*, 309, L7
 Granot, J., Piran, T., & Sari, R. 1999, *ApJ*, 527, 236
 Gruzinov, A. 1999, *ApJ*, 525, L29
 Katz, J. I. 1994, *ApJ*, 432, L107
 Landau, L. D., & Lifshits, E. M. 1975, *The classical theory of fields, Course of theoretical physics, v. 2* (New York: Pergamon Press)
 Liang, E. P., Kusunose, M., Smith, I. A., & Crider, A. 1997, *ApJ*, 479, L35
 Mazets, E. P., et al. 1981, *Nature*, 290, 378
 Medvedev, M. V., & Loeb, A. 1999, *ApJ*, 526, 697
 Mészáros, P. 1999, *astro-ph/9912475*
 Mészáros, P., & Rees, M. J. 1993, *ApJ*, 405, 278
 Murakami, T., et al. 1988, *Nature*, 335, 324
 Palmer, D. M., et al. 1994, *ApJ*, 433, L77
 Panaitescu, A., & Mészáros, P. 1998, *ApJ*, 493, L31
 Papatthanassiou, H. 1999, *A&AS*, 138, 525
 Pendleton, J. N., et al. 1994, *ApJ*, 431, 416
 Piran, T. 1999, *Phys. Rep.*, 314, 575
 Preece, R. D., Briggs, M. S., Malozzi, R. S., Pendleton, G. N., Paciesas, W. S., & Band, D. L. 1998, *ApJ*, 506, L23
 Rees, M.J., & Mészáros, P. 1994, *ApJ*, 430, L93
 Ryde, F. 1999, *astro-ph/9910204*
 Rybicki, G. B., & Lightman, A. P. 1979, *Radiative processes in astrophysics*, (New York: Wiley)
 Sari, R. 1999, *ApJ*, 524, L43
 Sari, R. 1998, *ApJ*, 494, L49
 Sari, R., Narayan, R., & Piran, T. 1996, *ApJ*, 473, 204
 Schaefer, B. E., et al. 1998, *ApJ*, 492, 696
 Strohmer, T. E., Fenimore, E. E., Murakami, T., & Yoshida, A. 1998, *ApJ*, 500, 873
 Wijers, R. A. M. J., & Galama, T. J. 1998, *ApJ*, 523, 177
 Wijers, R. A. M. J., et al. 1999, *ApJ*, 523, L33